The Electrochemical Corrosion of Bulk Nanocrystalline Aluminum in Acidic Sodium Sulfate Solutions at Room Temperature

ARTICLE *in* THE JOURNAL OF PHYSICAL CHEMISTRY C · APRIL 2015

Impact Factor: 4.77 · DOI: 10.1021/acs.jpcc.5b00904

5 AUTHORS, INCLUDING:

S.G. Wang

Chinese Academy of Sciences

34 PUBLICATIONS **478** CITATIONS

THE JOURNAL OF PHYSICAL CHEMISTRY C

Article

pubs.acs.org/JPCC

Electrochemical Corrosion of Bulk Nanocrystalline Aluminum in Acidic Sodium Sulfate Solutions at Room Temperature

S. G. Wang,* Y. J. Huang, M. Sun, K. Long, and Z. D. Zhang

Shenyang National Laboratory for Material Sciences, Institute of Metal Research, Chinese Academy of Sciences, 72 Wenhua Road, 110016 Shenyang, P. R. China

ABSTRACT: The corrosion properties of metallic materials are usually associated with the compactness of the oxide film and electrochemical parameters, such as corrosion potential, corrosion current density, pitting potential, etc. The valence electron configurations of metallic materials can also affect their corrosion properties because the nature of their corrosion processes involves the exchange and transportation of valence electrons between metallic atoms and ions. In the present work, the electrochemical corrosion of bulk nanocrystalline aluminum (BN-Al) produced by severe rolling technique and its conventional polycrystalline aluminum (CP-Al) counterpart in 0.01, 0.05, and 0.1 M HCl + 0.25 M Na_2SO_4 solutions at room temperature was studied by potentiodynamic polarization, electrochemical impedance spectroscopy, and scanning electron microscopy. The uniform and pitting corrosion resistances of BN-Al were simultaneously enhanced in comparison with those of CP-Al. The ion adsorption in oxide films along depth profiles on BN-Al and CP-Al and their valence electron configurations were characterized by X-ray photoelectron spectroscopy and ultraviolet photoelectron spectroscopy, respectively. The enhanced corrosion resistance of BN-Al resulted from its valence electron configuration rather than the Cl^-, SO_4^{2-}, and Na^+ adsorptions and the oxide film on BN-Al.

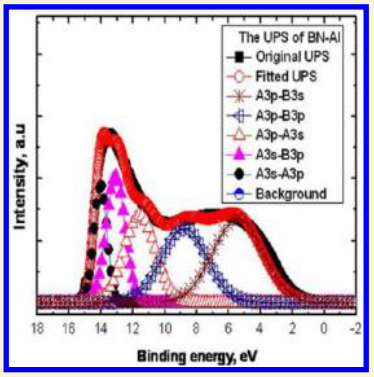

1. INTRODUCTION

The corrosion properties of Al and Al alloys with grain size from micrometer to nanometer scale have been studied extensively because of their applications in many fields due to their low density, high specific strength, and good resistance to uniform corrosion.[1−9] The introduction of huge plastic deformation by multipass equal-channel angular pressing (ECAP) to both Al-5.4 wt % Ni and Al-5 wt % Cu alloys increased pitting potential in a neutral buffer solution containing 0.002 M Cl^-, while pure Al after four passes of ECAP resulted in a decrease of open circuit potential, a slight increase of passive current, and a shift of pitting potential to the negative direction.[10] The low-alloy steel with a high Al content was imparted better passivation behavior resulting in a lower corrosion rate in a 10 wt % H_2SO_4 solution (pH 0.13).[11] The enhanced corrosion resistance in 3.5 wt % NaCl solution of ultrafine-grained Al-26 wt % Si alloy prepared by ECAP was attributed to the homogeneous ultrafine-grain structure with the breakage of brittle and large primary silicon crystals.[12] The resistance of sputtered microcrystalline Al coating to pitting corrosion was improved with increasing the concentration of F^- ions in NaF + NaCl aqueous solutions when the concentration of F^- was larger than that of Cl^-.[13] The corrosion resistance of microcrystalline Al coating fabricated by magnetron sputtering deteriorated more compared with that of the cast pure Al in Na_2SO_4 acidic solution. However, its oxide film had a higher pitting resistance in acidic NaCl solution.[14] The electrochemical corrosion behavior of 6061 Al alloy was found to depend on pH and chloride concentration.[15] For low chloride ion concentrations, 6056 Al alloy was less resistant to pitting than 2024 Al alloy, but it was opposite for the high chloride ion concentrations.[16] In the presence of SO_4^{2-} ions, passivity was extended over a wide potential range and breakdown of passivity occurred when the material was polarized beyond pitting potential.[17] The breakdown potentials and pit transition potentials of ultrafine-grained binary Al−Mg alloy prepared by ECAP slightly decreased, shifted to more negative value, and became deeper with increasing the pass number of ECAP.[18] The improvement of pitting corrosion resistance of anodized Al−Cu alloy prepared by ECAP was ascribed to a decrease in the size of precipitates.[19]

In the present work, the electrochemical corrosion of bulk nanocrystalline aluminum (BN-Al) and its conventional polycrystalline aluminum (CP-Al) counterpart in 0.01, 0.05, and 0.1 M HCl + 0.25 M Na_2SO_4 solutions at room temperature was studied by potentiodynamic polarization, electrochemical impedance spectroscopy (EIS), scanning electron microscope (SEM), and X-ray photoelectron spectroscopy (XPS). The valence electron configurations (such as the density of states distribution, binding energy (E_b), weights of valence electrons, and work function (ϕ_s)) of BN-Al and CP-Al were characterized by ultraviolet photoelectron spectroscopy (UPS). The electrochemical corrosion of BN-Al and CP-Al was explained according to their electrochemical corrosion parameters, the ion adsorption in the oxide films, and their valence electron configurations.

Received: January 28, 2015
Revised: March 8, 2015
Published: April 13, 2015

DOI: 10.1021/acs.jpcc.5b00904
J. Phys. Chem. C 2015, 119, 9851−9859

2. EXPERIMENTAL SECTION

2.1. Materials, Electrochemical Methods, and SEM Observation. Bulk nanocrystalline aluminum (BN-Al) was prepared by severe rolling technique. The details of this technique were described in our previous work.[20] The grain size of BN-Al was about 130 nm;[21] the chemical composition of BN-Al and the conventional polycrystalline aluminum counterpart were (wt %) Fe 0.5%, Si 0.45%, Cu 0.02%, Mg 0.05%, Mn 0.05%, remainder Al. BN-Al and CP-Al specimens ($10 \times 15 \times 1.0$ mm^3) were polished using SiC papers of successive grades up to 1200#, cleaned by distilled water, degreased with acetone, and then dried with hot air. The working areas of BN-Al and CP-Al in electrochemical tests are 10×10 mm^2. The electrochemical measurement of BN-Al and CP-Al in 0.01, 0.05, and 0.1 M HCl + 0.25 M Na_2SO_4 solutions was carried out at room temperature with an electrochemical workstation (CHI600C, Shanghai, China). Three-electrode jacketed test cells were used with a platinum foil as auxiliary electrode. A saturated KCl calomel electrode (SCE) coupled to a luggin capillary whose tip was located between the working electrodes was chosen as reference electrode. The frequency range for EIS measurement was set from 10^4 to 0.01 Hz. The amplitude of sinusoidal excitation voltage was 10 mV. The EIS data of BN-Al and CP-Al were analyzed by ZSimpWin 3.10 software. The scan range of potential for potentiodynamic polarization of BN-Al and CP-Al in the three kinds of solutions was −1.0−0.4 V (vs SCE); the scan rate was 0.33 mV/s because of the chemical activity of solutions (HCl + Na_2SO_4) and Al. The electrochemical parameters, such as corrosion current density, corrosion potential, and charge-transfer resistance, were obtained from potentiodynamic polarization and EIS. Each type of electrochemical measurement was repeated at least three times until good reproducibility of data was obtained. The morphologies of BN-Al and CP-Al corroded surfaces in the three kinds of solutions were observed by SEM (SSX-550, SHIMADZU, Japan) at 20 kV after these corroded surfaces were coated with gold.

2.2. Characterization of Ion Adsorption in the Oxide Film and Valence Electron Configurations of BN-Al and CP-Al. The ion adsorptions (Cl^-, Al^{3+}, SO_4^{2-}, and Na^+) in the oxide films along depth profiles on BN-Al and CP-Al were characterized by XPS (ESCALAB250 system). The base pressure of ESCALAB250 system was better than 2.8×10^{-10} Pa, and the XPS photons were from a monochromatic Al target (Kα line, 1486.6 eV). Pure Au and Ag standard samples were used to calibrate the binding energy by setting Au $4f_{7/2}$ and Ag $3d_{5/2}$ peaks at binding energies of 83.98 ± 0.02 eV and 368.26 ± 0.02 eV, respectively. The Fermi edge was calibrated using pure Ni and setting the binding energy at 0.00 ± 0.02 eV. Depth profiling in the oxide films on BN-Al and CP-Al was performed over an area of 2.0×2.0 mm^2 under Ar^+ sputtering with 2 keV. Ar^+ sputtering time during XPS measurement was 2400 s for both BN-Al and CP-Al. The valence electron configurations of BN-Al and CP-Al were characterized by UPS (He I $h\nu$ = 21.22 eV, ± 0.05 eV, ESCALAB250) after Ar^+ sputtering for 300s to obtain clear surfaces. BN-Al and CP-Al were biased at −3.0 V during UPS measurement to observe the low cutoff of secondary electron, E_c, and obtain the work function, ϕ_s. The UPS of BN-Al and CP-Al, composition analysis, and background subtraction of the high-resolution XPS of O(O^{2-} + O^0) 1s and Al(Al^{3+} + Al^0) $2p_{3/2}$ were analyzed by XPSPEAK4.1 software.

3. RESULTS

3.1. Electrochemical Corrosion. Panels a, b, and c of Figure 1 show potentiodynamic polarization plots of BN-Al and CP-Al in 0.01, 0.05, and 0.1 M HCl + 0.25 M Na_2SO_4 solutions,

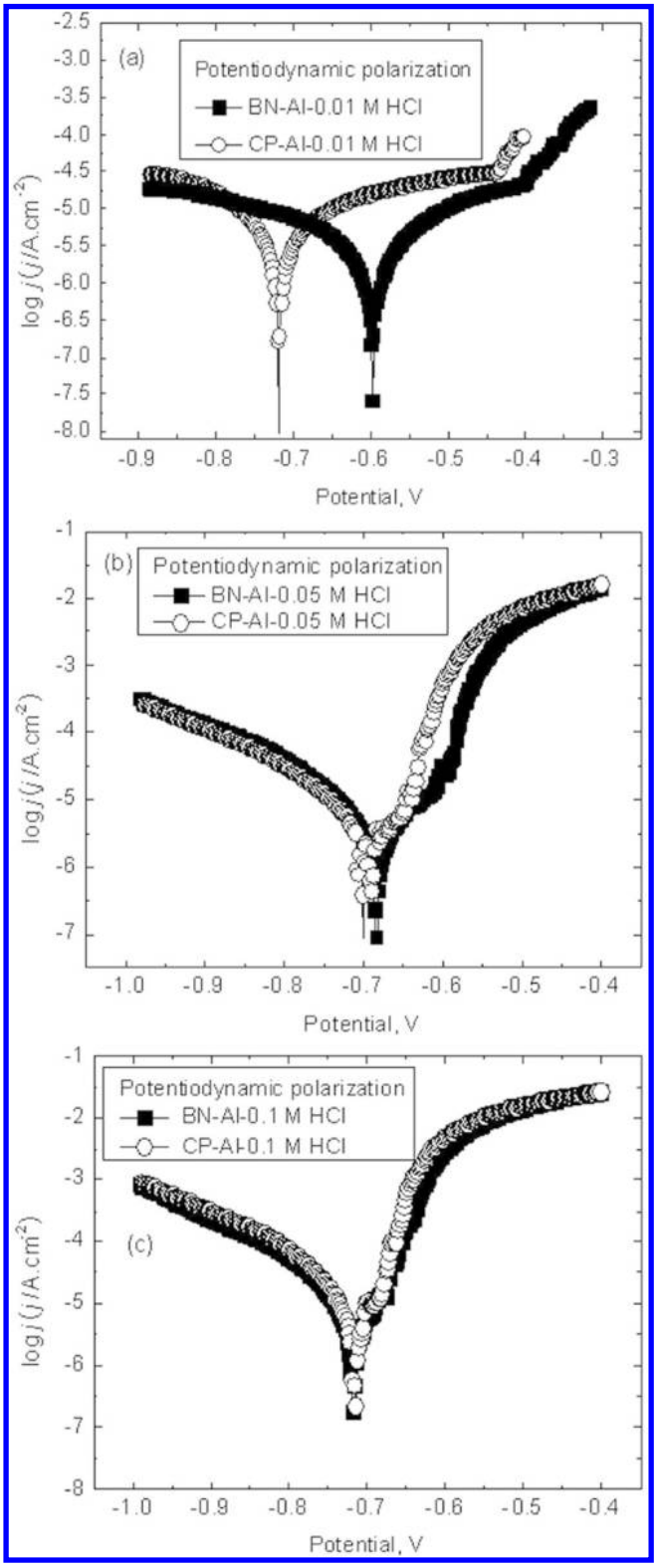

Figure 1. Potentiodynamic polarization of BN-Al and CP-Al with scan rate at 0.33 mV/s in 0.01 M (a), 0.05 M (b), and 0.1 M (c) HCl + 0.25 M Na_2SO_4 solutions at room temperature.

DOI: 10.1021/acs.jpcc.5b00904
J. Phys. Chem. C 2015, 119, 9851−9859

respectively. The electrochemical parameters of potentiodynamic polarization are listed in Table 1. The corrosion current densities, I_{corr}, of BN-Al and CP-Al increased with the concentration of hydrochloric acid, while the I_{corr} of BN-Al was less than that of CP-Al for the same concentration of hydrochloric acid. The corrosion potentials, E_{corr} (vs SCE), of BN-Al and CP-Al became more negative with increasing concentration of hydrochloric acid, but E_{corr} of BN-Al was more positive than that of CP-Al in the same concentration of HCl. Panels a and b of Figure 2 present the EIS of BN-Al and CP-Al in 0.01 and 0.05 M HCl + 0.25 M Na_2SO_4 solutions, respectively. The EIS of BN-Al and CP-Al in 0.1 M HCl + 0.25 M Na_2SO_4 solution can not be provided because the concentration of HCl is too high to maintain a stable potential for EIS measurement. Figure 2c represents the equivalent circuit of EIS in Figure 2. The EIS parameters (R_s, R_{ct}, R_0, Y_0, n, and L) of BN-Al and CP-Al in Figure 2 for BN-Al and CP-Al in 0.01 and 0.05 M HCl + 0.25 M Na_2SO_4 solutions are listed in Table 2. R_s represents the solution resistance. Constant phase element Q is used in place of a capacitor to compensate the nonhomogeneity, which is defined by two values, Y_0 and n. If n is equal to 1, Q is identical to a capacitor. R_t denotes charge-transfer resistance. R_0 and L represent the inductance resistance and inductance, respectively, which are used to describe the low-frequency inductance loop, implying pitting corrosion and adsorption. For the same HCl concentration, R_{ct}, R_0, Y_0 and L of BN-Al were larger than those of CP-Al, respectively.

Table 1. Potentiodynamic Polarization Parameters of BN-Al and CP-Al in HCl (0.01, 0.05, and 0.1M) + 0.25 M Na_2SO_4 Solutions

solution	E_{corr} (mV)		I_{corr} (μA/cm^2)	
HCl + Na_2SO_4	BN-Al	CP-Al	BN-Al	CP-Al
0.01 M + 0.25 M	−597	−718	3.72	8.57
0.05 M + 0.25 M	−684	−701	1.85	2.24
0.1 M + 0.25 M	−716	−717	4.15	6.50

3.2. Corroded Surface Morphologies. Figure 3a−f shows the corroded surface morphologies of BN-Al and CP-Al in 0.01, 0.05, and 0.1 M HCl + 0.25 M Na_2SO_4 solutions. In Figure 3a,b, both BN-Al and CP-Al did not evidently suffer from pitting corrosion in 0.01 M HCl + 0.25 M Na_2SO_4 solution due to the low concentration of hydrochloric acid and high concentration of SO_4^{2-}, which agrees with the potentiodynamic polarization in Figure 1a that indicated there was no fluctuation in the anodic polarization of BN-Al and CP-Al. However, BN-Al and CP-Al evidently suffered from pitting corrosion in 0.05 and 0.1 M HCl + 0.25 M Na_2SO_4 solutions as revealed from Figure 3c−f, which is consistent with the potentiodynamic polarization shown in Figure 1b,c in which there are obvious fluctuations in the anodic polarization of BN-Al and CP-Al. In Figure 3c−f, the larger density of pitting corrosion on CP-Al in the same concentration of hydrochloric acid means that its pitting corrosion resistance was degraded in comparison with that of BN-Al.

3.3. Ion Adsorption on Oxide Films. Figure 4a−d shows the atomic percentages of Na^+ and S^{6+} (in SO_4^{2-}) in oxide films along depth profiles on BN-Al and CP-Al. There was almost no Na^+ in the oxide films along depth profiles on BN-Al in the three kinds of solutions and on CP-Al in 0.01 M HCl + 0.25 M Na_2SO_4 solution, whereas the atomic percentages of Na^+ changed from 2.7% to 0.5% in the oxide films along depth profiles on CP-Al in 0.05 and 0.1 M HCl + 0.25 M Na_2SO_4 solutions (Figure 4a). In the 0.01 M HCl + 0.25 M Na_2SO_4 solution, the atomic percentages of S^{6+} in the oxide film along depth profile on CP-Al were larger than those on BN-Al, while the atomic percentage differences of S^{6+} in the oxide films along depth profiles between BN-Al and CP-Al were only within 2.0% as observed from Figure 4b. In 0.05 M HCl + 0.25 M Na_2SO_4 solution, the largest atomic percentage difference of S^{6+} adsorption between BN-Al and CP-Al was about 3.2% on their top corroded surfaces (without Ar^+ sputtering), but the S^{6+} atomic percentages in the oxide film along depth profile on BN-Al were almost the same as those on CP-Al according to Figure 4c. In 0.1 M HCl + 0.25 M Na_2SO_4 solution, the largest atomic percentage difference of S^{6+} between BN-Al and CP-Al was about 7.8% on their top corroded surfaces, while the atomic percentages of S^{6+} in the oxide film along depth profile on BN-Al were also almost equal to those on CP-Al, as seen from Figure 4d. Panels a, b, and c of Figure 5 illustrate the atomic percentages of Cl^- in the oxide films along depth profiles on BN-Al and CP-Al in 0.01, 0.05, and 0.1 M HCl + 0.25 M Na_2SO_4 solutions, respectively. The atomic percentage differences of Cl^- between BN-Al and CP-Al were only within 1%, which means that there were no significant difference of Cl^- adsorption between BN-Al and CP-Al.

Panels a and b of Figure 6 denote for the atomic percentages of Al (Al^{3+} + Al^0) and O (O^{2-} + O^0) in the oxide films along depth profiles on BN-Al and CP-Al in the three kinds of solutions, respectively. The atomic percentages of Al (Al^{3+} + Al^0) in the oxide film along depth profile on CP-Al in 0.1 M HCl + 0.25 M Na_2SO_4 solution were smaller than those on CP-Al in 0.01 and 0.05 M HCl + 0.25 M Na_2SO_4 solutions and those on BN-Al in the three kinds of solutions. The atomic percentages of Al (Al^{3+} + Al^0) in the oxide films along depth profiles on BN-Al in the three kinds of solutions were very close to those on CP-Al in 0.01 and 0.05 M HCl + 0.25 M Na_2SO_4. The atomic percentages of O (O^{2-} + O^0) in the oxide film along depth profile on CP-Al in 0.1 M HCl + 0.25 M Na_2SO_4 were larger than those on CP-Al in 0.01 and 0.05 M HCl + 0.25 M Na_2SO_4 solutions and those on BN-Al in the three kinds of solutions. The atomic percentages of O (O^{2-} + O^0) in the oxide films along depth profiles on BN-Al in the three kinds of solutions were almost the same as those on CP-Al in 0.01 and 0.05 M HCl + 0.25 M Na_2SO_4 solutions, as shown in Figure 6b.

3.4. Valence Electron Configurations. The electronic structures and valence band structures of oxide films can be characterized by XPS and UPS.[22] UPS also can characterize the valence electron configuration of metallic materials.[23,24] Figure 7a,b shows the UPS of BN-Al and CP-Al at room temperature. The original UPS of BN-Al and CP-Al were fitted by five peaks: A3s-A3p, A3s-B3p, A3p-A3s, A3p-B3p, and A3p-B3s. A3s, A3p, B3s, and B3p represent valence electrons 3s and 3p of Al atoms A and B respectively. In Figure 8, the arrows 1−5 denote the interactions of different valence electrons in different orbits for Al atoms A and B. There are no interactions between valence electrons $3p^1$ and $2s^2$ (for different atoms) because of the shield of $3s^2$ orbit, and no interactions between valence electrons $2p^6$ and $2s^2$ because of the occupied $2p^6$ and $2s^2$ (for the same atom). The work functions ϕ_s can be obtained according to the following equation

$$\varphi_s = h\nu + E_c - E_F \quad (1)$$

E_F is the Fermi levels of BN-Al and CP-Al. ϕ_s of BN-Al and CP-Al are 4.63 and 4.41 eV, respectively, and ϕ_s of BN-Al is 0.22 eV larger than that of CP-Al. The E_b and weights of the five valence electron peaks of BN-Al and CP-Al are listed in Table 3. The E_b

DOI: 10.1021/acs.jpcc.5b00904
J. Phys. Chem. C 2015, 119, 9851−9859

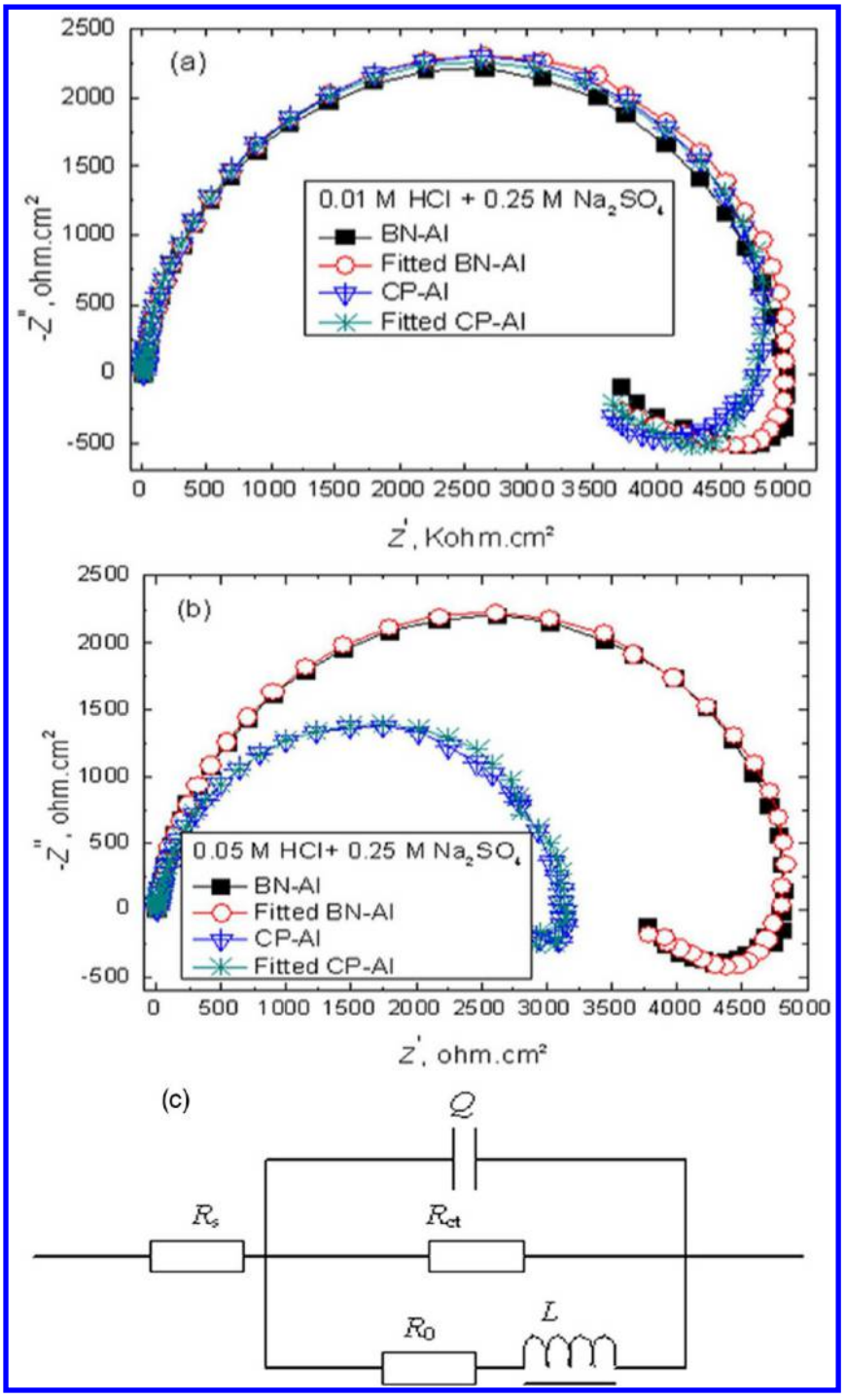

Figure 2. Electrochemical impedance spectroscopy of BN-Al and CP-Al in 0.01 M (a) and 0.05 M (b) HCl + 0.25 M Na_2SO_4 solutions at room temperature and their equivalent circuit (c).

Table 2. EIS Parameters of BN-Al and CP-Al in 0.01 and 0.05 M HCl + 0.25 M Na_2SO_4 Solutions

	R_s		R_{ct} (ohm cm^2)		R_0 (ohm cm^2)		CPE-Y_0 ($\times 10^{-5}$)		CPE-n		L (H cm^{-2})	
HCl	BN	CP	BN	CP	BN	CP	BN	CP	BN	CP	BN	CP
0.01 M	12.41	13.25	5313	5067	1549	1381	2.11	2.12	0.93	0.93	6806	4762
0.05 M	13.76	11.71	4955	3217	1704	1209	2.15	2.86	0.92	0.91	5536	4665

values of the five valence electron peaks of BN-Al were larger than those of the corresponding valence electron peaks of CP-Al. There is almost no difference between the weights of the corresponding five valence electron peaks of BN-Al and CP-Al.

4. DISCUSSION

Figure 1 and Table 1 demonstrate the lower corrosion current density and more positive corrosion potential of BN-Al in comparison with those of CP-Al in the three kinds of solutions.

DOI: 10.1021/acs.jpcc.5b00904
J. Phys. Chem. C 2015, 119, 9851−9859

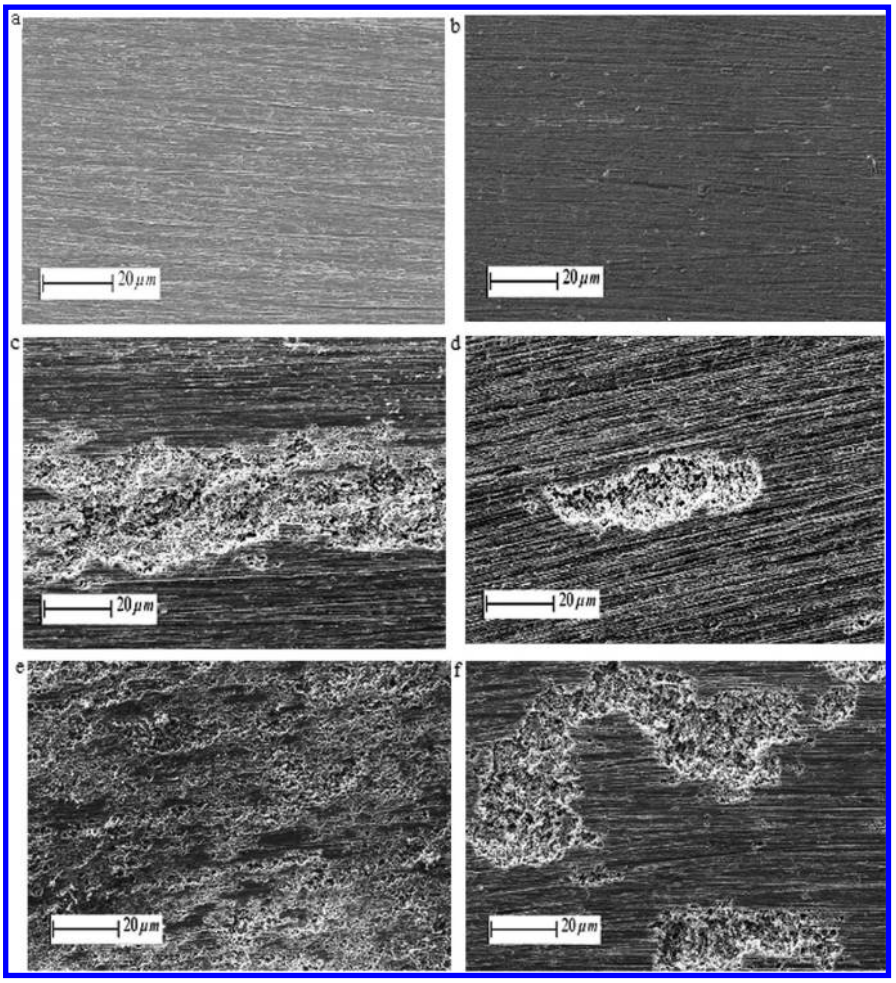

Figure 3. Morphologies of BN-Al and CP-Al corroded surfaces at room temperature: CP-Al in 0.01 M (a), 0.05 M (C), and 0.1 M (e) HCl + 0.25 M Na_2SO_4 solutions; BN-Al in 0.01 M (b), 0.05 M (d), and 0.1 M (f) HCl + 0.25 M Na_2SO_4 solutions.

The charge-transfer resistances of BN-Al were larger than those of CP-Al in 0.01 and 0.05 M HCl + 0.25 M Na_2SO_4 solutions according to Figure 2 and Table 2. Figure 3a,b indicates that there was no evident pitting corrosion on BN-Al and CP-Al. Therefore, the uniform corrosion resistance of BN-Al was enhanced in 0.01 M HCl + 0.25 M Na_2SO_4 solution according to Figures 1a, 2a, and 3a,b. Figure 3c−f and Tables 1 and 2 indicate that the pitting corrosion resistances of BN-Al were improved in comparison with CP-Al in 0.05 and 0.1 M HCl + 0.25 M Na_2SO_4 solutions. Therefore, Figures 1−3 demonstrate that the uniform and pitting corrosion resistances of BN-Al were simultaneously enhanced in comparison with those of CP-Al at room temperature.

The corrosion resistance of metallic material is associated with the chemisorptive interactions on its surface.[25] The following facts can be derived from Figures 4 and 5: (1) The stronger Na^+, SO_4^{2-}, and Cl^- adsorption did not occur on BN-Al in the three kinds of solutions. (2) The SO_4^{2-} adsorption on CP-Al and BN-Al top surfaces became stronger and almost independent of the concentration of hydrochloric acid, respectively, while the SO_4^{2-} adsorption in oxide films on BN-Al and CP-Al were very weak and scarcely associated with the concentration of hydrochloric acid, respectively. (3) The Cl^- and Na^+ adsorptions on the top surface of the oxide film on BN-Al were also weak and did not depend on the concentration of hydrochloric acid. (4) The Na^+ adsorption in the oxide film on CP-Al became stronger with the concentration of hydrochloric acid. (5) The same Cl^- adsorption occurred in the oxide films on BN-Al and CP-Al in the three kinds of solutions and did not depend on the concentration of hydrochloric acid.

It should be noted that the atomic percentages of O^0 and Al^{3+} will decrease with Ar^+ sputtering because the atomic percentage of Al^0 will increase with Ar^+ sputtering because the thinner oxide film can result in the larger possibility of being probed by XPS for metallic substrate. Figure 6 indicates the same thickness and compactness of oxide films on BN-Al and CP-Al in 0.01 and 0.05 M HCl + 0.25 M Na_2SO4 solutions, and on BN-Al in 0.1 M HCl + 0.25 M Na_2SO4 solution due to the same atomic percentages of Al (Al^{3+} + Al^0) and O (O^{2-} + O^0) along the depth profile during Ar^+ sputtering. The oxide film on CP-Al in 0.1 M HCl + 0.25 M Na_2SO_4 solution was the thickest and the most compact among all the oxide films on BN-Al and CP-Al because of the lowest atomic percentage of Al (Al^{3+} + Al^0) and the largest atomic percentage of O (O^{2-} + O^0), as shown in Figure 6. In Figures 1−3, the current densities of BN-Al and CP-Al are the sum of the current densities of polarization and the chemical reaction between oxide film and HCl solution. The weights of current densities of the chemical reaction between oxide film and HCl solution became larger with the increment of HCl concentration. The weight of current densities of the chemical reaction between oxide film and HCl solution in Figure 1c should be the largest among Figure 1a−c because of the largest concentration of HCl.

DOI: 10.1021/acs.jpcc.5b00904
J. Phys. Chem. C 2015, 119, 9851−9859

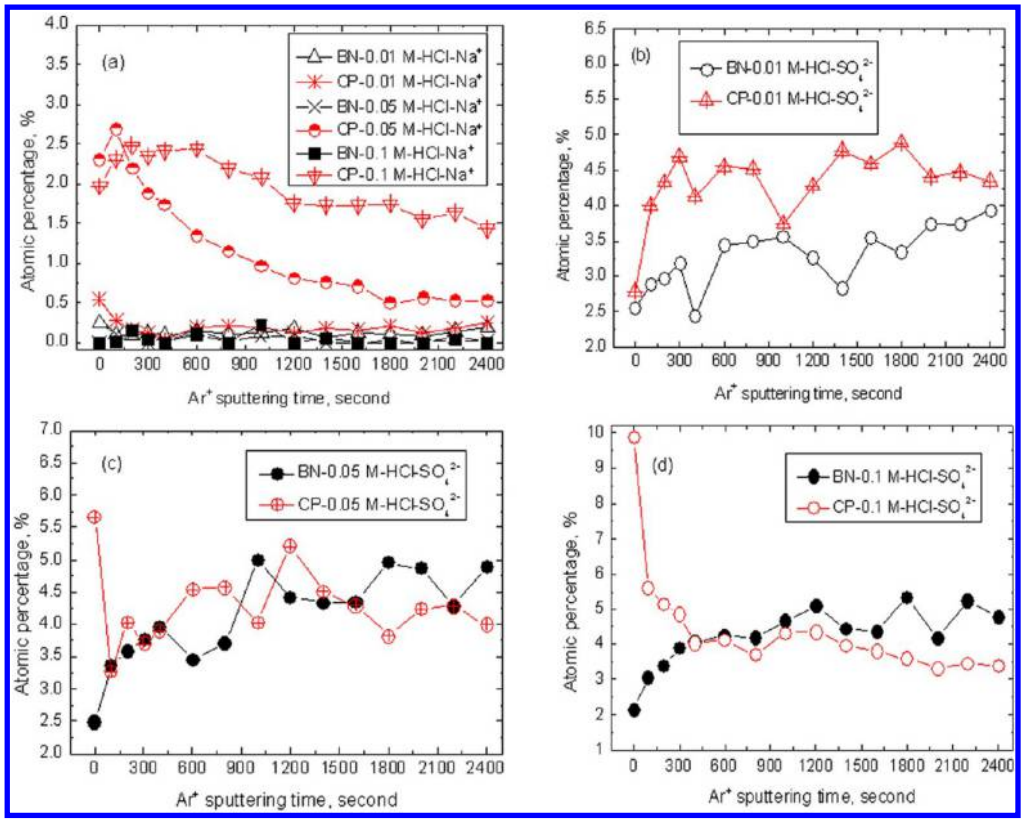

Figure 4. Atomic percentages of Na^+ (a) and SO_4^{2-} (b–d) on BN-Al and CP-Al in 0.01, 0.05, and 0.1 M HCl + 0.25 M Na_2SO_4 solutions at room temperature.

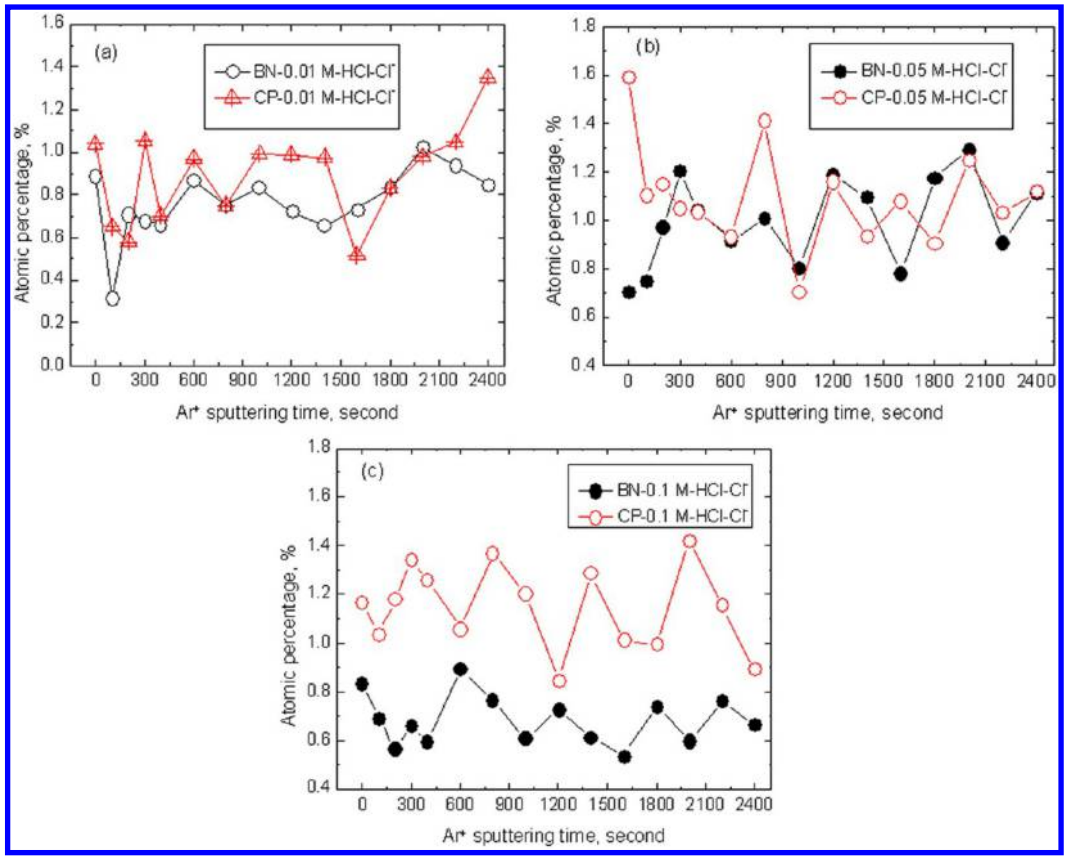

Figure 5. Atomic percentages of Cl^- on BN-Al and CP-Al in 0.01 M (a), 0.05 M (b), and 0.1 M (c) HCl + 0.25 M Na_2SO_4 solutions at room temperature.

DOI: 10.1021/acs.jpcc.5b00904
J. Phys. Chem. C 2015, 119, 9851–9859

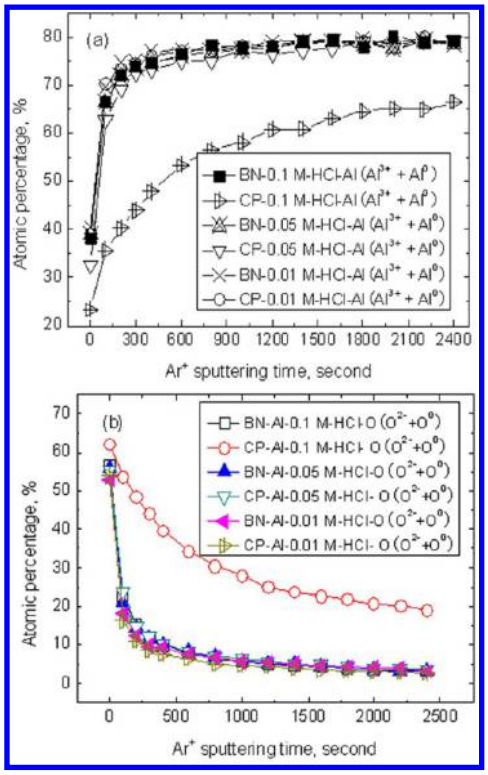

Figure 6. Atomic percentages of Al (Al^{3+} + Al^0) (a) and O (O^{2-} + O^0) (b) on BN-Al and CP-Al in 0.01, 0.05, and 0.1 M HCl + 0.25 M Na_2SO_4 solutions at room temperature.

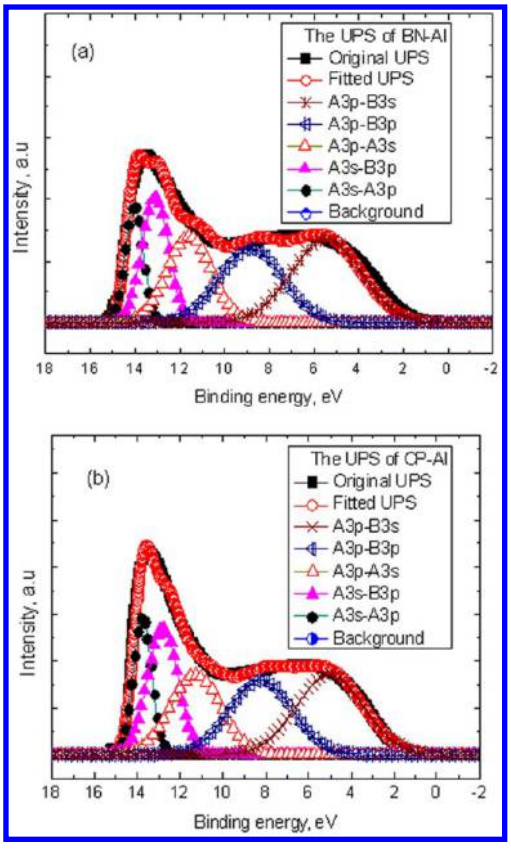

Figure 7. Ultraviolet photoelectron spectroscopy of BN-Al (a) and CP-Al (b).

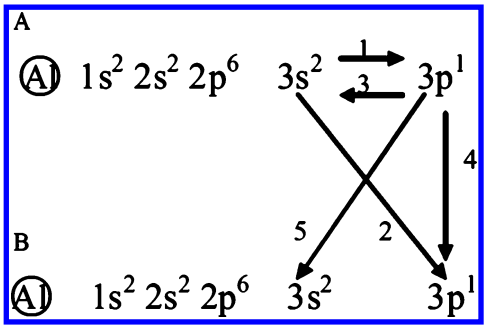

Figure 8. Schematic illustration of the interaction between the valence electrons of Al atoms.

Table 3. Binding Energies and Weights of Valence Electrons of BN-Al and CP-Al[a]

	A3s-A3p	A3s-B3p	A3p-A3s	A3p-B3p	A3p-B3s
E_b-BN (eV)	14.02	13.08	11.57	8.80	5.43
E_b-CP (eV)	13.76	12.82	11.28	8.24	5.01
W-BN (%)	10.65	16.83	19.34	23.62	29.55
W-CP (%)	12.31	19.01	19.67	22.73	26.28

[a] E_b-BN and E_b-CP denote the E_b of valence electrons of BN-Al and CP-Al, respectively. *W*-BN and *W*-CP represent the weights of valence electrons of BN-Al and CP-Al respectively.

Therefore, the actual current densities (so-called polarization behaviors in Figure 1c) of BN-Al and CP-Al may become increasingly similar as the solution became more acidic and almost coincided at 0.1 M HCl + 0.25 M Na_2SO_4 solution. How to evaluate the contribution of the chemical reaction between oxide film and HCl solution to current density in Figures 1 is very interesting work; we will carry out further investigation regarding this topic in the future.

Generally, the enhanced uniform and pitting corrosion resistances of metallic materials are attributed to thicker and more compact oxide films,[12,26−31] higher SO_4^{2-} concentration (stronger SO_4^{2-} adsorption), and lower Cl^- concentration (weaker Cl^- adsorption) on the corroded surface.[15−17] Although the thickness, compactness, and atomic percentages of elements along the depth profile of the oxide film on CP-Al were the same as those on BN-Al in 0.01 and 0.05 M HCl + 0.25 Na_2SO_4 solutions, the uniform and pitting corrosion resistances of BN-Al were improved simultaneously according to Figures 1−6 and Tables 1 and 2. The weaker SO_4^{2-} adsorption, same Cl^- adsorption, smaller thickness of oxide film, and same compactness of oxide film occurred on BN-Al in comparison with those on CP-Al in 0.1 M HCl + 0.25 M Na_2SO_4 solution according to Figures 3−6. However, the uniform and pitting corrosion resistances of BN-Al were also simultaneously improved in 0.1 M HCl + 0.25 Na_2SO_4 solution at room temperature. In contrast, the strong SO_4^{2-} adsorption and the thicker oxide films occurred on CP-Al, while the uniform and pitting corrosion resistances of CP-Al were degraded in comparison with those of BN-Al at room temperature. Therefore, the thicker oxide film and the stronger SO_4^{2-} adsorption cannot result in improving the corrosion resistance; the enhanced uniform and pitting corrosion resistances of BN-Al resulted from BN-Al material itself rather than the thicker and more compact oxide film, stronger SO_4^{2-} adsorption, and weaker Cl^- adsorption on it.

One usually studies the corrosion properties and their mechanisms of metallic materials by electrochemical methods[1−9] and in situ observations (such as in situ electro-

DOI: 10.1021/acs.jpcc.5b00904
J. Phys. Chem. C 2015, 119, 9851−9859

chemical scanning tunneling microscopy[31] and in situ X-ray absorption spectroscopy[32]), and these methods mainly focus on the dynamic processes of corrosion.[33] In fact, the nature of electrochemical corrosion is the exchange and transportation processes of valence electrons between atoms or ions.[23,24,34,35] Therefore, the valence electron configurations (such as work function, the density of states distribution of valence electrons, and binding energies of valence electrons) of metallic materials are among the intrinsic parameters to affect the exchange processes at atomic scale because of the following facts: (1) The larger work function results in the larger resistance of valence electron away from metallic substrate; the surface reactivity or corrosion behavior of a metal is intrinsically determined by the work function.[36−39] (2) The larger binding energies of valence electrons with the same density of states distribution can result in the smaller possibility for changing a metallic atom to a cation. Therefore, the larger work function of BN-Al and the larger binding energies of valence electrons with the same density of states distribution of BN-Al as shown in Table 3 were the main factors for its enhanced uniform and pitting corrosion resistances in the three kinds of solutions at room temperature. The severe rolling deformation enhanced the interactions of valence electrons between different atoms and the interaction between different valence electrons in the same atom. This is the main factor for studying the valence electron configurations of BN-Al and CP-Al and the adsorption of ions in oxide films rather than the conventional microstructures (such as dislocation density and residual strain) of BN-Al and CP-Al.

5. CONCLUSION

Both the uniform and pitting corrosion resistances of BN-Al were simultaneously improved in comparison with those of CP-Al in 0.01, 0.05, and 0.1 M HCl + 0.25 M Na_2SO_4 solutions at room temperature. The oxide films on BN-Al were not thicker than those on CP-Al; the oxide films on CP-Al were not less compact than those on BN-Al. The Na^+ adsorption in the oxide films and the SO_4^{2-} adsorption on the top surfaces of oxide films on CP-Al were stronger than those on BN-Al, and the Cl^- adsorption in oxide films on BN-Al was the same as that on CP-Al in the three kinds of solutions. The stronger SO_4^{2-} adsorption and thicker oxide films on CP-Al did not result in the enhanced corrosion resistance of CP-Al in 0.1 M HCl + 0.25 M Na_2SO_4 solution. The improved uniform and pitting corrosion resistances of BN-Al mainly resulted from its larger work function and its larger binding energies of valence electrons rather than the SO_4^{2-} adsorption and the thickness and compactness of oxide films on BN-Al. The stronger SO_4^{2-} adsorption cannot cause larger corrosion resistance in any case.

AUTHOR INFORMATION

Corresponding Author

*E-mail: sgwang@imr.ac.cn. Tel.: +86-24-83978750. Fax: +86-24-23891320.

Notes

The authors declare no competing financial interest.

ACKNOWLEDGMENTS

The authors are grateful to the financial support of Natural Sciences Foundation of China, Contract 51171199, and the National Basic Research Program (2010CB934603) of China, Ministry of Science and Technology China.

REFERENCES

(1) Li, J. F.; Maier, B.; Frankel, G. S. Corrosion of an Al−Mg−Si Alloy Under $MgCl_2$ Solution Droplets. *Corros. Sci.* **2011**, *53*, 2142−2151.
(2) Amin, M. A.; Abd El Rehim, S. S.; El-Lithy, A. S. Pitting and Pitting Control of Al in Gluconic Acid Solutions − Polarization, Chronoamperometry and Morphological Studies. *Corros. Sci.* **2010**, *52*, 3099−3108.
(3) Serna, L. M.; Zavadil, K. R.; Johnson, C. M.; Wall, F. D.; Barbour, J. C. A Critical Implanted Cl^- Concentration for Pit Initiation on Aluminum Thin Films. *J. Electrochem. Soc.* **2006**, *153*, B289−B295.
(4) Amin, M. A.; Abd El Rehim, S. S.; El-Lithy, A. S. Corrosion, Passivation and Breakdown of Passivity of Al and Al-Cu Alloys in Gluconic Acid Solutions. *Electrochim. Acta* **2010**, *55*, 5996−6003.
(5) Eizadjou, M.; Fattahi, H.; Talachi, A. K.; Manesh, H. D.; Janghorban, K.; Shariat, M. H. Pitting Corrosion Susceptibility of Ultrafine Grains Commercially Pure Aluminium Produced by Accumulative Roll Bonding Process. *Corros. Eng., Sci. Technol.* **2012**, *47*, 19−24.
(6) Gupta, G.; Birbilis, N.; Cook, A. B.; Khanna, A. S. Polyaniline-lignosulfonate/epoxy Coating for Corrosion Protection of AA2024-T3. *Corros. Sci.* **2013**, *67*, 256−267.
(7) Amin, M. A. Metastable and Stable Pitting Events on Al Induced by Chlorate and Perchlorate Anions-Polarization, XPS and SEM Studies. *Electrochim. Acta* **2009**, *54*, 1857−1863.
(8) Gupta, R. K.; Hinton, B. R. W.; Birbilis, N. The Effect of Chromate on the Pitting Susceptibility of AA7075-T651 Studied Using Potentiostatic Transients. *Corros. Sci.* **2014**, *82*, 197−207.
(9) Lashgari, M.; Kianpour, E.; Mohammadi, E. Aluminum Pitting Corrosion in Halide Media: A Quantum Model and Empirical Evidence. *J. Mater. Eng. Perform.* **2013**, *22*, 3620−3625.
(10) Akiyama, E.; Zhang, Z. G.; Watanabe, Y.; Tsuzaki, K. Effects of Severe Plastic Deformation on the Corrosion Behavior of Aluminum Alloys. *J. Solid State Electrochem.* **2009**, *13*, 277−282.
(11) Nam, N. D.; Kim, W. C.; Kim, J. G. Effect of Aluminum on the Corrosion Resistance of Low-Alloy Steel in 10 wt% Sulfuric Acid Solution. *Mater. Corros.* **2012**, *63*, 1004−1010.
(12) Jiang, J. H.; Ma, A. B.; Song, D.; Yang, D. H.; Shi, J.; Wang, K. L.; Zhang, L. Y.; Chen, J. Q. Anticorrosion Behavior of Ultrafine-Grained Al-26 wt% Si Alloy Fabricated by ECAP. *J. Mater. Sci.* **2012**, *47*, 7744−7750.
(13) Zhang, B.; Li, Y.; Wang, F. H. Electrochemical Behaviour of Microcrystalline Aluminum in Neutral Fluoride Containing Solution. *Corros. Sci.* **2009**, *51*, 268−275.
(14) Zhang, B.; Li, Y.; Wang, F. H. Electrochemical Corrosion Behaviour of Microcrystalline Aluminium in Acidic Solutions. *Corros. Sci.* **2007**, *49*, 2071−2082.
(15) Zaid, B.; Saidi, D.; Benzaid, A.; Hadji, S. Effects of pH and Chloride Concentration on Pitting Corrosion of AA6061 Aluminum Alloy. *Corros. Sci.* **2008**, *50*, 1841−1847.
(16) Blanc, C.; Mankowski, G. Susceptibility to Pitting Corrosion of 6065 Aluminum Alloy. *Corros. Sci.* **1997**, *39*, 949−959.
(17) Datta, J.; Bhattacharya, C.; Bandyopadhyay, S. Influence of Cl, Br, NO_3^- and SO_4^{2-} Ions on the Corrosion Behavior of 6061 Al Alloy. *Bull. Mater. Sci.* **2005**, *28*, 253−258.
(18) Brunner, J. G.; May, J.; Hoppel, H. W.; Goken, M.; Virtanen, S. Localized Corrosion of Ultrafine -Grained Al-Mg Model Alloys. *Electrochim. Acta* **2010**, *55*, 1966−1970.
(19) Son, I. J.; Nakano, H.; Oue, S.; Kobayashi, S.; Fukushima, H.; Horita, Z. Pitting Corrosion Resistance of Anodized Aluminum-Copper Alloy Processed by Severe Plastic Deformation. *Mater. Trans.* **2008**, *49*, 2648−2655.
(20) Wang, S. G.; Shen, C. B.; Long, K.; Yang, H. Y.; Wang, F. H.; Zhang, Z. D. Preparation and Electrochemical Corrosion Behavior of Bulk Nanocrystalline Ingot Iron in HCl Acid Solution. *J. Phys. Chem. B* **2005**, *109*, 2499−2503.
(21) Wang, S. G.; Huang, R. J.; Mei, Y.; Long, K.; Li, L. F.; Zhang, Z. D. The Linear Thermal Expansion of Bulk Nanocrystalline Al and SS304 at Low Temperature. *Phys. B (Amsterdam, Neth.)* **2011**, *406*, 2758−2762.

DOI: 10.1021/acs.jpcc.5b00904
J. Phys. Chem. C 2015, 119, 9851−9859

(22) Cakir, P.; Eloirdi, R.; Huber, F.; Konings, R. J. M.; Gouder, T. An XPS and UPS Study on the Electronic Structure of ThO_x ($x \leq 2$) Thin Films. *J. Phys. Chem. C* **2014**, *118*, 24497−24503.
(23) Wang, S. G.; Sun, M.; Long, K. The Enhanced Even and Pitting Corrosion Resistances of Bulk Nanocrystalline Steel in HCl Solution. *Steel Res. Int.* **2012**, *83*, 800−807.
(24) Wang, S. G.; Sun, M.; Long, K. The Electrochemical Corrosion of Bulk Nanocrystalline Ingot Iron in HCl Solutions with Different Concentrations. *Mater. Chem. Phys.* **2011**, *127*, 459−463.
(25) Oguzie, E. E.; Adindu, C. B.; Enenebeaku, C. K.; Ogukwe, C. E.; Chidiebere, M. A.; Oguzie, K. L. Natural Products for Materials Protection: Mechanism of Corrosion Inhibition of Mild Steel by Acid Extracts of Piper Guineense. *J. Phys. Chem. C* **2012**, *116*, 13603−13615.
(26) Akhoondan, M.; Sagues, A. A. Corrosion Mechanism of Aluminized Steel in Limestone Backfill. *Corrosion (Houston, TX, U.S.)* **2013**, *69*, 1147−1157.
(27) Jayaraj, J.; Shankar, A. R.; Mudali, U. K. Electrochemical and Passive Characterization of a Beta Type $Ti_{45}Zr_{38}Al_{17}$ Cast Rod in Nitric Acid Medium. *Electrochim. Acta* **2012**, *85*, 210−219.
(28) Song, D.; Ma, A. B.; Jiang, J. H.; Lin, P. H.; Shi, J. Improving Corrosion Resistance of Pure Al Through ECAP. *Corros. Eng. Sci. Technol.* **2011**, *46*, 505−512.
(29) Xu, R. Z.; Yang, X. B.; Suen, K. W.; Wu, G. S.; Li, P. H.; Chu, P. K. Improved Corrosion Resistance on Biodegradable Magnesium by Zinc and Aluminum Ion Implantation. *Appl. Surf. Sci.* **2012**, *263*, 608−612.
(30) Zhang, J. F.; Zhang, W.; Yan, C. W.; Du, K. Q.; Wang, F. H. Corrosion Behaviors of Zn/Al-Mn Alloy Composite Coating Deposited on Magnesium Alloy ZA31B (Mg-Al-Zn). *Electrochim. Acta* **2009**, *55*, 560−571.
(31) Martinez-Lombardia, E.; Maurice, V.; Lapeire, L.; Graeve, I. D.; Verbeken, K.; Kestens, L.; Marcus, P.; Terryn, H. In Situ Scanning Tunneling Microscopy Study of Grain-Dependent Corrosion on Microcrystalline Copper. *J. Phys. Chem. C* **2014**, *118*, 25421−25428.
(32) Seo, M.; Fushimi, K.; Aoki, Y.; Habazaki, H.; Inaba, M.; Yokomizo, M.; Hayakawa, T.; Nakayama, T. *In situ* X-ray Absorption Spectroscopy for Identification of Lead Species Adsorbed on a Nickel Surface in Acidic Perchlorate Solution. *J. Electroanal. Chem.* **2012**, *671*, 7−15.
(33) Natishan, P. M.; Mccafferty, E.; Hubler, G. K. The Corrosion Behavior of Mo-Al, Cr-Al and Cr-Mo-Al Surface Alloys Produced by Ion-beam Mixing and Ion-implantation. *Corros. Sci.* **1991**, *32*, 721−731.
(34) Wang, S. G.; Sun, M.; Han, H. B.; Long, K.; Zhang, Z. D. The High-Temperature Oxidation of Bulk Nanocrystalline 304 Stainless Steel in Air. *Corros. Sci.* **2013**, *72*, 64−72.
(35) Wang, S. G.; Sun, M.; Long, K.; Zhang, Z. D. The Electronic Structure Characterization of Oxide Film on Bulk Nanocrystalline 304 Stainless Steel in Hydrochloric Acid Solution. *Electrochim. Acta* **2013**, *112*, 371−377.
(36) Chen, C.; Li, D. Y.; Shang, C. J. Nanocrystallization of Aluminized Surface of Carbon Steel for Enhanced Resistances to Corrosion and Corrosive wear. *Electrochim. Acta* **2009**, *55*, 118−124.
(37) Tao, S. L.; Li, D. Y. Nanocrystallization Effect on the Surface Electron Work Function of Copper and Its Corrosion Behaviour. *Philos. Mag. Lett.* **2008**, *88*, 137−144.
(38) Neufeld, A. K.; Cole, I. S.; Bond, A. M.; Furman, S. A. The Initiation Mechanism of Corrosion of Zinc by Sodium Chloride Particle Deposition. *Corros. Sci.* **2002**, *44*, 555−572.
(39) Li, W.; Li, D. Y. Influence of Surface Morphology on Corrosion and Electronic Behavior. *Acta Mater.* **2006**, *54*, 445−452.

DOI: 10.1021/acs.jpcc.5b00904
J. Phys. Chem. C 2015, 119, 9851−9859